Seismic Q estimates in Umbria-Marche (central Italy): hints for the retrieval of a new attenuation law for seismic risk

Journal:	*Geophysical Journal International*
Manuscript ID:	GJI-S-14-0832.R2
Manuscript Type:	Research Paper
Date Submitted by the Author:	02-Feb-2015

Complete List of Authors:	Pisconti, Angelo; Università di Bari, Dipartimento di Scienze della Terra e Geoambientali Del Pezzo, Edoardo; Istituto Nazionale di Geofisica e Vulcanologia, Osservatorio Vesuviano Bianco, Francesca; INGV -Osservatorio Vesuviano-Istituto Nazionale di Geofisica e Vulcanologia, Seismology de Lorenzo, Salvatore; Università di Bari, Scienze della Terra e Geoambientali

Keywords:	Seismic attenuation < SEISMOLOGY, Computational seismology < SEISMOLOGY, Numerical approximations and analysis < GEOPHYSICAL METHODS

Seismic Q estimates in Umbria-Marche (central Italy): hints for the retrieval of a new attenuation law for seismic risk

Angelo Pisconti (*), Edoardo Del Pezzo(1,**), Francesca Bianco(**)and Salvatore de Lorenzo (*)

*Dipartimento di Scienze della Terra, Università di Bari “Aldo Moro”, Bari, Italy

** Istituto Nazionale di Geofisica e Vulcanologia, sezione di Napoli Osservatorio Vesuviano, Napoli, Italy

(1) also at InstitutoAndaluz de Geofisica, Universidad de Granada,Granada,Spain

corresponding author:
Salvatore de Lorenzo, via Orabona 4, 70125 Bari, Italy, email: salvatore.delorenzo@uniba.it

Abstract

In the Umbria Marche (Central Italy) region an important earthquake sequence occurred in 1997, characterized by nine earthquakes with magnitudes in the range between 5 and 6, that caused important damages and causalities. In the present paper we separately estimate intrinsic- and scattering- Q^{-1} parameters, using the classical MLTWA approach in the assumption of a half space model. The results clearly show that the attenuation parameters Qi^{-1} and Qs^{-1} are frequency dependent. This estimate is compared with other attenuation studies carried out in the same area, and with all the other MLTWA estimates obtained till now in other tectonic environments in the Earth. The bias introduced by the half space assumption is investigated through numerical solutions of the Energy Transport equation in the more realistic assumption of a heterogeneous crust overlying a transparent mantle, with a Moho located at a depth ranging between 35 and 45 km below the surface. The bias introduced by the half space assumption is significant only at high frequency. We finally show how the attenuation estimates, calculated with different techniques, lead to different PGA decay with distance relationships, using the well known and well proven Boore's method. This last result indicates that care must be used in selecting the correct estimate of the attenuation parameters for seismic risk purposes. We also discuss the reason why MLTWA may be chosen among all the other available techniques, due to its intrinsic stability, to obtain the right attenuation parameters.

Introduction

For a complete revision of the seismic risk studies, the detailed knowledge of local attenuation vs. distance relationship is fundamental, as it governs how the energy of seismic radiation decreases with distance. For risk purposes, the empirical ground motion amplitude (max displacement, velocity or acceleration)decay curve with distance, calculated from experimental data, is commonly taken as the characteristic attenuation-distance curve in the area under study. Being empirically determined (see e.g. Akkar and Bommer, 2010), such curves do not explicitly contain information about the attenuation mechanisms of the seismic energy, which, on the contrary, can be deduced by measurements based on a physical model of attenuation. Such a model should include scattering losses, due to the important effects of heterogeneity in modifying the primary wave field and in the same time producing a scattering wave field (Sato and Fehler, 1998). The importance of scattering attenuation resides in the fact that part of the (apparently) absorbed energy associated with direct (ballistic) waves is recuperated in the scattered waves, which in turn are associated with lapse times much longer than the direct wave travel times, thus constituting the coda of the seismograms.

The purpose of the present paper is to contribute to the formulation of the seismic hazard in the Umbria Marche region, with a novel estimate of the quality factor, Q. From a physical point of view, the wave energy decay for cycle ($-\Delta E/E$) is expressed in terms of the quality factor parameter, Q_T, in turn related to the attenuation coefficient, η, through the following equation:

$$-\Delta E/E = \frac{2\pi}{Q_T} = 2\pi\left(\frac{1}{Q_i} + \frac{1}{Q_S}\right) = \frac{v\eta}{f} \qquad (1)$$

where v is the wave speed, f is the frequency of the wave motion, Q_i and Q_S are respectively the intrinsic-and scattering-Q. It is noteworthy that, in general, Q_T depends on the wave type (P, S, Surface, coda). The physical mechanism of energy dissipation (intrinsic or scattering) determines which part of Q_T is associated with scattering or with intrinsic attenuation.

This effect is important and should be taken into account for seismic risk purposes too, as a high scattering attenuation on one hand reduces the amplitude of direct waves, while on the other hand makes the direct wave train longer, for the effect of scattering. This is the reason why, in the present paper, we face with a separate estimate of intrinsic and scattering quality factors, trying in this way to understand the attenuation mechanisms in the seismic region of Umbria-Marche (Central Italy). We first give a review of the already calculated estimates of the seismic quality factors in this region, and then re-estimate separately intrinsic-and scattering-Q using the theory of the elastic Energy Transfer and **Multiple Lapse Time Window Analysis** (MLTWA) method (**Fehler et al., 1992**). Then we evaluate the leakage effect of a transparent mantle, i.e. a mantle characterized by no scattering, through the numerical simulations obtained with a Montecarlo method (Yoshimoto, 2000). Finally we show how the different Q estimates produce different Peak Ground Acceleration (PGA) curves with distance in the area under study, enlightening the important role of the attenuation studies in the seismic risk assessment.

Seismological setting

The Umbria-Marche region (central Italy) is a seismically active region of the northern Apennines. A prolonged seismic crisis occurred in this area in 1997, with nine main-shocks having a magnitude higher than Mw = 5, and more than 2000 aftershocks (Amato et al., 1998).The seismicity in the area is generated by a complex fault system, related to several compressional and extensional tectonic phases (Pauselli et al., 2006). From the Oligocene to the present-day, the area has experienced two phases of eastward migrating deformation: an early compression with eastward directed thrusting and a later phase of extension (Pauselli et al., 2006). The 1997 seismic activity was recognized as due to tectonic activity along both a low-angle detachment fault, known as Alto Tiberina fault and associated antithetic faults (e.g. Chiaraluce et al., 2003). The spatial and temporal evolution of the 1997 Umbria–Marche seismic sequence was successfully modeled in terms of subsequent failures promoted by fluid flow (Miller et al., 2004; Antonioli et al., 2005). A fluid-filled separated crack system was also invoked to explain the polarization anomalies of S waves (de Lorenzo and Trabace, 2011).

After the 1997 seismic crisis, several episodes of prolonged seismic activity occurred in the area, indicating that the Umbria-Marche region is one of the most tectonically active zones of Apennines. To mitigate seismic hazard, it is therefore very important to assess how the seismic energy scales with the distance in the area. Previous seismic attenuation studies of the Umbria-Marche region have been carried out (**Del Pezzo and Zollo, 1984, Del Pezzo and Scarcella, 1986, Castro et al., 1998, Bindi et al., 2004, Castro et al., 2004,** de Lorenzo et al., 2010, 2013a, 2013b). In particular, de Lorenzo et al. (2010) inferred source and attenuation parameters under the assumption of a constant Q_P. They inferred an average Brune (1976) stress drop $\Delta\sigma_B = 7MPa$, and computed the following seismic moment M_0 vs.magnitude M_L relationship:

$$\log_{10} M_0 = 0.81 M_L + 11.85 \qquad (2)$$

where M_0 is measured in Nm.

de Lorenzo et al. (2013a) separated the frequency dependent intrinsic Q_i^{-1} and scattering Q_s^{-1} attenuation parameters for the Umbria-Marche region using the approach developed by Wennerberg (1993), that is based on the separate estimates of S-wave total-attenuation coefficient and Q-coda attenuation. These authors also estimated coda attenuation Q_c^{-1}, using the isotropic single-scattering model (Sato,1977), and the shear wave attenuation Q_β^{-1}, using the coda normalization method (Aki, 1980). By comparing the Q estimates for the investigated area with those of other tectonically active regions of the world, obtained using the same approach, it was inferred that the Umbria-Marche region is characterized by higher values of Q_c^{-1}, Q_s^{-1} and Q_i^{-1}. It is noteworthy that the Wennerberg (1993) approach assumes that source and receiver are co-located, with no correction for site effects. As a consequence, this method furnishes reasonable but rough estimates only when the S wave travel time from the source to receiver is smaller as compared to the lapse times considered in the analysis (de Lorenzo et al. 2013a). To overcome the limits of the previous analysis, in this article we use the MLTWA technique, that implicitly takes into account the site effects, combined with the energy formulation due to Paaschens (1997), to remove the limitation of source and co-located receiver due to the Wennerberg (1993) approach. The previously obtained results are reported in table I.

Data, Technique and Results

The MLTWA technique (Fehler et al., 1992) is the most used method to separate the contribution of scattering and intrinsic attenuation on the seismic radiation. The method is based on the comparison between the observed and the theoretical seismic energy envelope in three fixed time windows following the S-wave arrival. To remove source intensity and site effects, the energy density is normalized to the energy content of a coda window of the same **duration** of the signal windows and starting at a given lapse time, the same for all the seismograms, calculated starting from the origin time (Aki, 1980).

The seismic energy envelope as a function of the lapse time and the distance, in a homogeneous half-space, can be modeled using the Energy Transport equation (Ishimaru, 1978) whose (approximate) analytical solution in 3-D is given by Paasschens (1997) (Formula 6 in Appendix), that describes the energy decay with lapse time and distance, implicitly including multiple isotropic scattering of any order. In the Paasschens solution, the density energy depends on two frequency dependent model parameters, the seismic albedo B_0, and the extinction length L_e. These two parameters can be expressed as a linear combination of Q_i and Q_s (see Formula 7 and 8 in Appendix).

In this study, we consider a dataset composed of 621 small magnitude earthquakes($1.4 \leq M_L \leq 4.4$) recorded by a mixed (permanent and temporary) array during the 1997 Umbria-Marche seismic crisis (figure 1). The network included 15 temporary and eight permanent stations. Ten temporary stations consisted of MarsLite data loggers recording on 230 Mbyte optical disks, in continuous mode at 125 samples per second (blue triangles in figure 1); four of them were equipped with Lennartz LE-3D/5s (flat velocity response between0.2 and 40 Hz) and six with Lennartz LE-3D/1s (flat velocity response between 1 and 40 Hz). Five temporary stations (red triangles in figure 1) consisted of RefTek 72-A07 data loggers equipped with Mark-L22-3D/1s (flat velocity response between 1 and 40 Hz). Permanent stations were managed by the RSM (Osservatorio Geofisico Sperimentale di Macerata) and RESIL (Regione Umbria) and recorded in continuous mode at 62.5 samples per second (squares and diamonds in figure 1). These stations consisted of MARS88/FD data loggers equipped with Mark L4C-3D seismometers (flat response between 1 and 40 Hz).

Of the available 621 earthquakes, 343 were used in a previous coda attenuation study (de Lorenzo et al., 2013a) for a total number of about 6500 three-component traces, spanning a source to receiver distance approximately ranging from 5 km to 65 km. **First of all**, these data were corrected for the instrument transfer function.

Owing to the dependence of Q on frequency, the following four frequency bands were considered: $1 \le f_c(Hz) \le 2$, $2 \le f_c(Hz) \le 4$, $4 \le f_c(Hz) \le 8$, $8 \le f_c(Hz) \le 16$.

Signals were bandpass filtered in each frequency band using a four poles Buttherworth filter, with cut-off frequencies at the extremes of any frequency band.

The MS (mean squared) envelope of each trace was preliminarily visualized (figure 2) in order to remove from the dataset those signals that are characterized by the presence of bumps in the considered time windows. As previously observed by de Lorenzo et al. (2013a), these bumps are mostly due to the time overlapping of the energy generated by two earthquakes that are separated in time of a quantity smaller than the total time window considered in the analysis. Since the maximum S-wave travel time is about equal to 20 s after the origin time and we used a total time window of 36 s, we discarded data having bumps in a window of 56 s after the origin time of the earthquake. After this analysis, the number of available three-component signals reduced to about 1800.

A further selection of data was carried out on the basis of the signal to noise ratio. We removed from the dataset all waveforms having an average signal <S> to noise <N> ratio less than 3, where <S> was estimated by the average level of absolute amplitude of the coda normalization window, whereas <N> was computed on a window preceding the P wave arrival. The results of this analysis are summarized in figure 3. We note that <S>/<N> generally decreases with increasing frequency. After this further selection of data, the number of available waveforms reduced to 384.

We then considered three consecutive time windows, having a width $\Delta t = 12$ s, starting from the S-wave arrival (figure 2) and a fourth window in the coda interval between 40 and 52 s from the origin time of the earthquake.

Since the shear waves are mostly pronounced onto the horizontal components, we considered only the two N-S and E-W components of the ground motion. In each time window, we finally calculated the time integral of the squared sum of the envelopes of the two horizontal components. After correcting for geometrical spreading, we thus write:

$$E_k^{obs}(r_i) = \log_{10} 4\pi r_i^2 \frac{\int_k (A_E^2 + A_N^2)dt}{\int_{40}^{52} (A_E^2 + A_N^2)dt} \qquad (3)$$

where A_E and A_N are the velocity envelopes in the K-th window for the i-th waveform, of the east and north component, respectively,

The values $E_K^{obs}(r_i)$ vs. r_i are shown in figure 4. The scatter of data is generally higher for the first considered time window, as observed in other tectonic areas (e.g. Del Pezzo et al., 2011). This effect is usually explained in terms of uncorrected radiation pattern effects; it is most important in the first time window, i.e. that following the S wave arrival, where the signal is dominated by the S-wave energy trapped around the recording site. For higher lapse times the signal is instead dominated by scattering effects, resulting in a smoother trend of observed data.

Following Del Pezzo et al. (2011), the fit of model to data was evaluated by computing the values of the following L2-norm misfit function:

$$M\left(L_e^{-1}, B_0\right) = \sum_{i=1}^{N}\sum_{k=1}^{3}\left[E_k^{obs}(r_i) - E_k^{theo}\left(r_i, L_e^{-1}, B_0\right)\right]^2 \qquad (4)$$

over a regular grid of the two-dimensional $\left(L_e^{-1}, B_0\right)$ parameter space. In equation (4), $E_k^{theo}\left(r_i, L_e^{-1}, B_0\right)$ is the theoretical normalized energy computed at the same distance r_i and in the same K-th time window of data. In our calculations, following Meirova and Pinsky (2014) we used a grid step for the extinction length $\Delta L_e^{-1} = 0.001$ km^{-1} in the range $0.003 \le L_e^{-1} \le 0.12$ km^{-1} and a grid step for the seismic albedo $\Delta B_0 = 0.01$ in the range $0.05 \le B_0 \le 0.95$. The minimum of the function (4) corresponds to the best fit values $\hat{L}_e^{-1}$ and $\hat{B}_0$. The error estimates on the best fit values $\hat{L}_e^{-1}$ and $\hat{B}_0$ were obtained by computing the isolines of the variable $M_{Norm} = M\left(L_e^{-1}, B_0\right) / M\left(\hat{L}_e^{-1}, \hat{B}_0\right)$. It has been shown that M_{Norm} is a F-variable (e.g. Mayeda et al., 1992; Del Pezzo and Bianco, 2010a) with N-2 degree of freedom, where N is the number of available data. The model parameters having a confidence level higher than a fixed threshold F*=0.68 are shown in figure 5. The estimate of model parameters and their errors are summarized in table II.

Q_i^{-1} and Q_s^{-1} are plotted vs. frequency in figure 6 and compared with the estimates of Q_i^{-1} and Q_s^{-1} previously obtained by de Lorenzo et al. (2013a). Smaller values of both intrinsic and scattering attenuation are inferred using MLTWA. The difference may be caused by the different assumptions of the two approaches. In particular, the assumption of a source co-located with the receiver (Sato, 1977), used in de Lorenzo et al. (2013a), could give rise to an overestimation of attenuation parameters, in that the source to receiver distances are maximized under this assumption.

In figure 7 we show most of the Q_i^{-1} and Q_s^{-1} MLTWA estimates, performed worldwide in the assumption of multiple scattering in half-space. It is worth noting that the Umbria-Marche region is characterized by one of the highest values of intrinsic attenuation, being Q_i^{-1} pattern with frequency in the upper bound of the values reported in figure 7. In de Lorenzo et al.(2013a) an equivalent results was found, by comparing the worldwide estimates obtained with the method described in Wennerberg (1993). Therefore, the present results confirm the interpretation in terms of pore fluid pressure affecting the inelastic properties of the crust. It has in fact been shown that intrinsic attenuation is the seismological attribute most sensitive to the physical state of the rocks and to fluid percolation (see e.g. de Lorenzo et al. (2001) and references therein). However, the thrust and fold belt representing the Apennine chain is characterized by small values of geothermal gradient (Mongelli et al., 2006) indicating that fluid percolation, from known deep sources (Miller et al., 2004; Chiodini et al., 2004), has to be responsible for the observed values of intrinsic attenuation.

MLTWA in a depth dependent model

Another point that has been addressed concerns the effect of the energy leakage caused by a transparent ($\eta_s = 0$) mantle (Margerin et al., 1998) on the inferred estimates of Q_i^{-1} and Q_s^{-1}. This is because the actual estimates of attenuation, obtained under the assumption of a homogeneous half-space, could be overestimated with respect to a depth dependent model (Del Pezzo and Bianco, 2010b). To account for the energy leakage caused by the mantle, we computed the numerical energy density curves in a two layered medium (crust over mantle), using a Montecarlo method (Yoshimoto, 2000). Since the Moho is at a depth of about 35-45 km in the area (Piana Agostinetti et al., 2002; Di Stefano et al., 2009), in the numerical simulations we considered three different velocity models (Moho depth respectively of 35, 40 and 45 km). Following Del Pezzo and Bianco (2010b), in each of these three models, the velocity of S waves is gradually enhanced from the crustal value (Vs=3.5km/s) to the mantle value (Vs=4.6km/s) in a thin layer around the Moho (figure 8), but the depth at which this transition occurs is different for the three models (35, 40 and 45 km).

The numerical curves are then compared with the averaged MLTWA data, regularized by computing their average values and standard deviations in distance intervals of 5 km **(Figure 9)**. To each data, a standard deviation equal to the average value of the standard deviations in each distance bin is associated.

In a first calculation, we assumed that the crust is characterized by the same Q_i^{-1} and Q_s^{-1} values inferred in the previous section under the assumption of a homogeneous half-space. Figure 9 shows the comparison of the numerical curves to data (solid colored lines and black points, respectively) **in the case of a Moho located at 40 km of depth**. The matching of the theoretical curves to data is quantified through the calculation of the significance level of a chi-square test. The results of a chi-square test indicate that the depth-dependent model satisfy the null hypothesis at a level of significance equal to 99% in the frequency band [1,2] Hz, that reduces to 0.2% in the frequency band [2,4] Hz and to 0.01 % in the frequency bands [4,8] Hz and [8-16] Hz. This indicates that only in the [1,2] Hz frequency band the Q_i^{-1} and Q_s^{-1} half-space estimates are not influenced by energy leakage in the mantle.

In a second calculation we evaluated how the crustal values of Q_i^{-1} and Q_s^{-1} have to be modified to obtain a good matching between model and data in the assumption of a transparent mantle. To this aim, we carried out a trial and error approach, that was stopped when the theoretical curves matched the data at a level of significance equal to 99 %. The results, obtained considering the three above described velocity models, are summarized in table III. The numerical curves for a depth dependent model that match the data are shown in figure 9 (red curves). The maximum difference between the depth dependent Q_i^{-1} and Q_s^{-1} values and the homogeneous model estimates is of the order of about 25%. We can conclude that the influence of the coda energy leakage into the mantle is not dramatic, in particular at low frequency. This result is probably the consequence of both the crustal thickening in the Umbria-Marche region and the small depth of considered earthquakes (average depth 3.7 km). Therefore, in a continental crust where shallow earthquakes occur, small bias in the attenuation estimates are obtained when considering a homogenous medium instead of a two-layered medium.

PGA attenuation with distance

To evaluate how different **Q estimates** reflect differences in the prediction of ground motion in the Umbria-Marche region, we simulate the peak ground acceleration for possible **total-Q values** taken from measurements done using different approaches. We use three different estimates of Q reported in Castro et al.(2002) (two of them achieved using the spectral decay method and the other using the Q-coda method) and the present MLTWA **estimate of** total-Q for S-waves, all obtained using similar data sets. The results are then compared with those found by Bindi et al. (2006), who report empirically retrieved PGA and PGV attenuation-distance relationships for Umbria-Marche.

To simulate the PGA values as a function of distance we use the method first developed by Boore (1983), in which the peak ground acceleration (PGA) (or the peak ground velocity, PGV) for a given earthquake magnitude is estimated using the random vibration theory (see also Boore, 2003). As described in Galluzzo et al.(2004), the present procedure is based on the Parseval–Plancherel theorem, which relates the **RMS** of a time series to its power spectrum. From the velocity or acceleration theoretical spectrum, corresponding to the Brune (1970) model, we calculate the **RMS**.

Then, we generate a set of **N** Gaussian distributed random numbers (**N**=2000) **with standard deviation, σ, equal to RMS** and take the maximum of this set as an estimate of the maximum acceleration (PGA). We used an Earth density of **3.0 × 10$^{\mathbf{3}}$** kg/m^3, a **S-wave** velocity of **3500 m/s**, a stress drop value for the area under study equal to its average value $\Delta\sigma = 7$ MPa (de Lorenzo et al., 2010), a source with a seismic moment of **3.5 ×10$^{\mathbf{16}}$ Nm**, corresponding to a M_L = **5.0** earthquake (equation 2), and a corner frequency, fc, equal to **0.8** Hz. **Source duration, Ts, was simply estimated by the inverse corner frequency. This parameter is crucial in the inference of PGA absolute value and should be empirically measured for the area under study, but in the present paper the actual aim is to compare the PGA pattern vs. distance obtained for different Q estimates, and not the absolute values. For the same above reason, we do not consider differences in the site attenuation at different distances, and arbitrarily chose a unique k-parameter (Anderson and Hough, 1984), setting it at 0.05 s, as previously inferred (Rovelli et al.,1998; Malagnini and Hermann, 2000) . In Table IV the parameters used in the simulations are summarized.**

We run the simulation for each attenuation relationship, for a set of source-receiver distance spanning a distance interval of 50 km. In figure 10 we plot the pattern of PGA values as a function of distance, together with their fit to the following relationships (see Kramer 1996, page 88 for a wide discussion on the empirical relationship describing peak acceleration decay with distance):

$$\mathrm{Log}[PGA] = a + bM + cM^2 + dR + f\mathrm{Log}[R] \qquad (5)$$

where a, b, c, d and f are parameters to be determined by the fit; M is the earthquake magnitude and R is the distance. **As can be seen by the plots in figure 10, with increasing the source to receiver distance, the simulated PGA curves, obtained using different Q estimates, tend to assume different values. In particular the simulations marked with #1 and #3 (Q estimates of Castro et al., 2002) differ by the simulation marked with #2 (Castro et al. 2002). The simulation marked with #2 predicts a PGA pattern similar to those inferred using the four Q-values estimated in this paper with the MLTWA technique. The errors on the model parameters**

obtained from the fit of equation 5 to simulated data are of the order of 10%, indicating that, with the exception of curves #1 and #3, the other curves are not statistically different. This indicates the importance of correctly choosing the proper measure of the quality factor for application purposes.

In the same plot, the empirical PGA vs. distance curve, determined by Bindi et al.(2006) for the same area, is reported for comparison. **Despite the indetermination in the estimate of ground motion duration in the present approach, it** matches most of the curves determined utilizing the Boore method with the attenuation parameters estimated in the present paper and the curves by Castro et al. (2002) **[except curve #1 and #3 for increasing distances]** in the distance range between 5 and **10 km**. **At shortest distances the curve by Bindi et al. (2006) slightly diverges from the pattern of PGA curves calculated using the Boore method**. This **(minor)** effect can be due to the point source assumption implicit in the development of the present simulation with the Boore's method and, possibly, in neglecting non linear or near field effects.

5 Concluding remarks

We have reviewed **almost** all the already obtained estimates of the seismic attenuation in the area of Central Italy (reported in Table I), and have applied the MLTWA technique to a large data set of local earthquakes in the same area in order to obtain a new estimate of intrinsic-and scattering-Q (Qi and Qs) from which a new estimate of total-Q, Q_T for S-waves has been inferred. For the sake of clarity, we note that Q_T obtained with MLTWA **(table II)** coincides with the direct total quality factor of S-waves Q_β measured with techniques different from MLTWA **(see table I)**.The present result evidences that, in the studied area, the heterogeneities which generate the scattering phenomena play an important role in determining the attenuation of the seismic waves only at low frequency, below 2 Hz, while intrinsic dissipation prevails for frequencies higher than 2 Hz. The contrary occurs in volcanoes, where scattering phenomena prevail over the intrinsic dissipation in determining the attenuation of the seismic energy with distance. **This is probably due to the high**

amount of heterogeneities in the composition of volcanoes.

The bias introduced by the half space assumption has been tested with numerical simulations. Owing to the high crustal thickness combined with the shallowness of sources, the coda energy leakage into the mantle is not important, indicating that the MLTWA estimates obtained in the present paper can be usefully utilized for seismic risk purposes, in order to deduce the correct attenuation laws for the prediction of the seismic ground motion.

Appendix

The radiative transfer or transport equation is an integral equation whose analytical solutions in 3 dimensions are not already known. An approximate analytical solution in 3-D was found by Paasschens (1997) in case of uniform half-space (constant velocity and scattering coefficient). It describes the pattern of the seismogram energy envelope, E[r, t], as a function of lapse timet; anddistance, r:

$$E[r,t] \approx \frac{W_0 \exp\left[-L_e^{-1} vt\right]}{4\pi r^2 v} \delta\left[t-\frac{r}{v}\right] +$$

$$W_0 H\left[t-\frac{r}{v}\right] \frac{\left[1-\frac{r^2}{v^2t^2}\right]^{1/8}}{\left[\frac{4\pi vt}{3B_0 L_e^{-1}}\right]^{3/2}} \exp\left[-L_e^{-1} vt\right] F\left[vtB_0 L_e^{-1}\left(1-\frac{r^2}{v^2t^2}\right)^{3/4}\right] \qquad (6)$$

where $F[x] = \mathrm{e}^{x}\sqrt{1+2.026/x}$, W_0 is the energy at source; v is the wave speed in the half-space; H is the Heaviside function; δ is the Dirac's delta, B_0 and Le^{-1} represent respectively the seismic albedo and the extinction length inverse, expressed in terms of Q_T by:

$$B_0 = \frac{Q_T}{Q_S} \qquad (7)$$

$$L_e^{-1} = \frac{2\pi f}{v}\left[\frac{1}{Q_s}+\frac{1}{Q_i}\right] \qquad (8)$$

Figure captions

Figure1. Geographic position of the seismic events and seismometers considered in this study.

Figure 2. An example of data processing. For both the EW and the NS component of a seismogram recorded at station CAS1 (a), the filtered signals in the 4-8 Hz range are computed (b). Of these signals the amplitude envelopes (c) and their squares (d) are computed. The density energy is computed on three 12 s time window of the signal representing the sum of the EW and NS squared envelopes (e).

Figure 3: Signal to noise ratio for the selected waveforms considered in this study, in the different frequency ranges. The grey line on each plot indicates the average value of <S/N> in each frequency band. Only data having <S/N>>3 are shown.

Figure 4. Plot of the normalized density energy vs. the source to receiver distance. Blue points refer to the first 12 s time window following the S wave arrival; red point refer to the second 12 s time window; green point refer to the third 12 s time window (see the text).Continuous line represent the theoretical best fit curves obtained in the assumption of homogenous half-space

Figure 5. Confidence region of model parameters at a significance level 68%. Blue area indicate the regions of acceptability of the F-test. The red points represent the best fit solution in each frequency band.

Figure 6. Comparison between Q_i^{-1} and Q_s^{-1} estimated in this study and their estimates with the Wennerberg (1993) method obtained by de Lorenzo et al. (2013).

Figure 7. Worldwide estimates of Q_i^{-1} and Q_s^{-1}. The colored symbols represents values of different Italian regions.

Figure 8. V_S velocity and scattering attenuation profiles used in the simulation with a depth-dependent attenuation model. Note that the scattering attenuation profiles are normalized by their crustal values, $\eta_{s,c}$.

Figure9. Fit to MLTWA data of the homogeneous (solid grey lines) and the depth dependent

attenuation model (blue and red solid lines). The chi-square values reported in each box refers to the uncorrected depth dependent model (see text, for more explanations).

Figure 10 . Pattern of PGA (simulated with the Boore's method) as a function of distance for different choices of attenuation parameters according to the following scheme:

1) $Q[f]=18 \cdot f^2$ in the range {1 -10 Hz}; Q[f]=990 for frequencies higher than 10 Hz (Spectral ratio method, Castro et al. 2002)

2) $Q[f]=34 \cdot f^{1.3}$(Spectral ratio method, Castro et al. 2002)

3) $Qc[f]=77 \cdot f^{0.6}$ (Q-coda method, Castro et al. 2002)

4) $Q[f]=25 \cdot f^{1.3}$(MLTWA method, this paper, Half Space)

5) $Q[f]=25 \cdot f^{1.3}$(MLTWA method, this paper, Moho Depth at 45 km)

6) $Q[f]=25 \cdot f^{1.3}$(MLTWA method, this paper, Moho Depth at 40 km)

7) $Q[f]=25 \cdot f^{1.4}$(MLTWA method, this paper, Moho Depth at 35 km)

Dashed black line is the empirical PGA-distance attenuation curve estimated by Bindi et al. (2006).

Table captions

Table I: Summary of previous attenuation studies in the Umbria-Marche region

Table II: MLTWA model parameter estimates in the half-space assumption

Table III: Results of the trial and error approach for the estimation of the attenuation parameters in the three considered depth dependent models. Results correspond to a level of significance of the χ-square test equal to 99%.

Table IV: Model parameters used in the simulations of the PGA values

References

Abubakirov, I.R., 2005. Attenuation characteristics of transverse waves in the Lithosphere of Kamchatka estimated from observations at the Petropavlovsk digital broadband station, *Izvestiya-Phys. Solid Earth*, **41**(10), 813–824.

Aki, K., 1980. Attenuation of shear-waves in the lithosphere for frequencies from 0.05 to 25 Hz,

Phys. Earth planet. Inter., **21**,50-60.

Akinci, A. & Eyidogan, H., 2000. Scattering and anelastic attenuation of seismic energy in the vicinity of north anatolian fault zone, eastern Turkey, *Phys. Earth planet. Inter.,* **122**(3-4), 229–239.

Akinci, A., Del Pezzo, E., & Ibanez, J., 1995. Separation of scattering and intrinsic attenuation in southern Spain and Western Anatolia (Turkey), *Geoph. J. Int.* **121**, 337–353.

Akkar, S., & Bommer, J.J., 2010. Empirical Equations for the Prediction of PGA, PGV, and Spectral Accelerations in Europe, the Mediterranean Region, and the Middle East, *Seism. Res. Lett.,* **81**(2), 195–206.

Amato, A., *et al.,* 1998. The 1997 Umbria-Marche, Italy, earthquake sequence: a first look at the main shocks and aftershocks, *Geophys. Res. Lett.,* **25,** 2861–2864.

Anderson, J.G., & Hough, S.E., 1984. A model for the shape of the Fourier amplitude spectrum of acceleration at high frequencies, *Bull. Seism. Soc. Am.*, **74**, 1969-1993.

Antonioli, A., Piccinini, D., Chiaraluce, L., & Cocco. M., 2005. Fluid flow and seismicity pattern: Evidence from the 1997 Umbria-Marche (central Italy) seismic sequence, *Geophys. Res. Lett.,* **32** (L10311), doi:10.1029/2004GL022256.

Badi, G., Del Pezzo, E., Ibanez, J.M., Bianco, F., Sabbione, N. & Araujo, M., 2009. Depth dependent seismic scattering attenuation in the Nuevo Cuyo region (southern central Andes), *Geophys.Res. Lett.,* **36**, L24307, doi:10.1029/2009GL041081.

Bianco, F., Del Pezzo, E., Castellano, M., Ibanez, J.M. & Di Luccio, F., 2002. Separation of intrinsic and scattering seismic attenuation in the southern Apennine zone, Italy, *Geophys. J. Int*., **150**, 10–22.

Bianco, F., Del Pezzo, E., Malagnini, L., Di Luccio, F. & Akinci, A., 2005. Separation of depth-dependent intrinsic and scattering seismic attenuation in the northeastern sector of the Italian Peninsula, *Geophys.J. Int.,* **161**(1), 130–142.

Bindi, D., Castro, R.R., Franceschina, G., Luzi,L., & Pacor, F., 2004. The 1997–1998 Umbria-Marche sequence (central Italy): Source, path, and site effects estimated from strong motion data recorded in the epicentral area, *J. Geophys. Res.,* 109, B04312, doi:10.1029/2003JB002857.

Bindi, D., Luzi, L., Pacor, F., Franceschina, G., & Castro. R.R., 2006. Groundmotion predictions from empirical attenuation relationships versus recorded data: The case of the 1997–1998 Umbria-Marche, central Italy, strong-motion data set, *Bull. Seism. Soc. Am.,* **96**(3), 984–1002.

Bindi, D., Parolai, S., Grosser, H., Milkereit, C., & Karakisa, S., 2006. Crustal attenuation characteristic in Northwestern Turkey in the range from 1 to 10 Hz, *Bull. Seism. Soc. Am.,* **96**, 200-214, doi: 10.1785/0120050038.

Bindi, D., Spallarossa, D., Augliera, P., & Cattaneo, M., 2001. Source parameters estimated from the aftershocks of the 1997 Umbria-Marche seismic sequence, *Bull. Seism. Soc. Am*., **91**, 448-455, doi:10.1785/0120000084.

Boore, D.M., 1983. Stochastic Simulation of High Frequency Ground Motions based on Seismological Models of the Radiated Spectra, *Bull. Seism. Soc. Am.,* **73**(6), 1865–1894.

Boore, D.M., 2003. Seismic Motion, Lithospheric Structures, Earthquake and Volcanic Sources*: The Keiiti Aki Volume*, Basel: Birkhäuser Basel.

Brune, J.N., 1970. Tectonic Stress and the Spectra of Seismic Shear Waves from Earthquakes. *J. Geophys. Res.,* **75**(26), 4997–5009.

Castro R. R., Monachesi, G., Mucciarelli, M., Trojani, L., & Pacor, F., 1999. P and S-wave attenuation in the region of Marche, Italy, *Tectonophysics*, *302, 123-132.*

Castro, R.R., Monachesi, G., Trojani, L., Mucciarelli, M., & Frapiccini, M., 2002. An attenuation study using earthquakes from the 1997 Umbria-Marche sequence, *J. Seismol.,* **6**(1), 43–59.

Castro, R.R., Pacor, F., Bindi, D., Franceschina, G., & Luzi, L., 2004. Site Response of Strong Motion Stations in the Umbria, Central Italy, Region, *Bull. Seismol. Soc. Am.*, 94, 576-590.

Chiaraluce, L., Ellsworth, W., Chiarabba, C., & Cocco, M., 2003. Imaging the complexity of an active normal fault system: The 1997 Colfiorito (central Italy) case study, *J. Geophys. Res.,* **108**(B6), doi:10.1029/2002JB002166.

Chiodini, G., Cardellini, C., Amato, A., Boschi, E., Caliro, S., Frondini, F., & Ventura, G., 2004. Carbon dioxide Earth degassing and seismogenesis in central and southern Italy, *Geophys. Res. Lett.,* **31**, L07615, doi:10.1029/2004GL019480.

Chung, T.W., Lees J.M., Yoshimoto, K., Fujita, K., & Ukawa, M., 2009. Intrinsic and scattering attenuation of the Mt Fuji Region, Japan, *Geophys. J. Int.,* **177**, 1366–1382.

de Lorenzo, S., Del Pezzo, E., & Bianco, F., 2013a. Qc, Q-beta, Qi and Qs attenuation parameters in the Umbria–Marche (Italy) region, *Phys. Earth planet. Inter.,* **218**, 19–30.

de Lorenzo, S., Bianco,F., & Del Pezzo, E., 2013b. Frequency dependent Q-alpha and Q-beta in the Umbria-Marche (Italy) region using a quadratic approximation of the coda-normalization method, *Geophys. J.Int.,* **193**(3), 1726–1731.

de Lorenzo, S. & Trabace, M., 2011. Seismic anisotropy of the shallow crust in the Umbria–Marche (Italy) region, *Phys. Earth planet. Int.,* **189**, 34–46.

de Lorenzo, S., Zollo, A., & Zito. G., 2010. Source, attenuation, and site parameters of the 1997 Umbria Marche seismic sequence from the inversion of P wave spectra: A comparison between constant QP and frequency dependent QP models, *J. Geophys. Res.,* **115**, B09306, doi:10.1029/2009JB007004.

de Lorenzo, S., Zollo, A., & Mongelli, F., 2001. Source parameters and three dimensional attenuation structure from the inversion of micro earthquake pulse width data: Qp imaging and inferences on the thermal state of the Campi Flegrei caldera (southern Italy), *J. Geophys. Res.*, **106**(B8), 16265–16286.

Del Pezzo, E. & Zollo, A., 1984. Attenuation of coda waves and turbidity coefficient in central Italy., *Bull. Seismol. Soc. Am.*, 74, 2655–2659.

Del Pezzo, E. & Scarcella, G., 1986. Three-component coda Q in the Abruzzi–Molise region, Central Apennines., *Ann. Geophys*., 4, 589–592.

Del Pezzo, E. & Bianco, F., 2010a. MathLTWA: Multiple lapse time window analysis using Wolfram Mathematica 7, *Computers and Geosciences,* **36**(10), 1388–1392.

Del Pezzo, E. & Bianco, F., (2010b). Two-layer earth model corrections to the MLTWA estimates of intrinsic-and scattering-attenuation obtained in a uniform half-space, *Geophys. J. Int.,* **182**(2), 949–955.

Del Pezzo, E., Bianco, F., Marzorati, S., Augliera, P., D'Alema, E., & Massa, M., 2011. Depth-dependent intrinsic and scattering seismic attenuation in north central Italy, *Geophys. J. Int.,* **186**(1), 373–381.

Di Stefano, R., Kissling, E., Chiarabba, C., Amato, A., & Giardini, D., 2009. Shallow subduction beneath Italy: three-dimensional images of the Adriatic–European–Tyrrhenian lithosphere system based on high-quality P wave arrival times, *J. Geophys. Res.* doi:10.1029/2008JB005641.

Dutta, U., Biswas, N.N., Adams, D.A., & Papageorgiou, A., 2004. Analysis of S-wave attenuation in South-Central Alaska, *Bull. Seism. Soc. Am.,* **94**, 16–28.

Fehler, M., Hoshiba, M., Sato, H., & Obara, O., 1992. Separation Of Scattering And Intrinsic Attenuation For The Kanto-tokai Region, Japan, Using Measurements Of S-wave Energy Versus Hypocentral Distance, *Geophys. J. Int.,* **108**(3), 787–800.

Galluzzo, D., Del Pezzo, E., La Rocca, M., & Petrosino, S., 2004. Peak ground acceleration produced by local earthquakes in volcanic areas of Campi Flegrei and Mt.Vesuvius, *Ann. Geophys*., **47**,1377-1389.

Giampiccolo, E., Tuve`, T., Gresta, S. & Patané, D., 2006. S-waves attenuation and separation of scattering and intrinsic absorption of seismic energy in southeastern Sicily (Italy), *Geophys. J. Int.,* **165**(1), 211–222.

Goutbeek, F.H, Dost, B, van Eck, T., 2004. Intrinsic absorption and scattering attenuation in the southern Netherlands, *J. Seismol.,* **8**, 11-23.

Ishimaru, A., (1978) *Wave Propagation and Scattering in Random Media,* Vols. 1 and 2. Academic Press, New York.

Jin, A., Mayeda, K., & Aki, K., 1994. Separation of intrinsic and scattering attenuation in southern California using TERRAscope data, *J. geophys. Res.,* **99**, 17835-17848.

Kramer, S.L., (1996, July). *Geotechnical Earthquake Engineering*, pp. 1–333.

Lee, W.S., Yun, S., & Do, J.Y., 2010. Scattering and intrinsic attenuation of short-period S waves in the Gyeongsang Basin, South Korea, revealed from S-wave seismogram envelopes based on the radiative transfer theory, *Bull. Seism. Soc. Am.*, **100**(2),833-840, doi 10.1785/0120090149.

Lemzikov, M.V., 2008. Estimation of shear-wave attenuation characteristics for the Klyuchevskoi volcanic edifice, *J. Volcanol. Seismol.,* **2**, 108–117.

Lemzikov, M.V., 2007. Intrinsic attenuation and scattering of shear waves in the lithosphere of Kamchatka, *J. Volc. Seismol.,* **1**(3), 185–197.

Malagnini, L. &. Herrmann R.B., 2000. Ground-Motion Scaling in the Region of the 1997 Umbria-Marche Earthquake (Italy), *Bull. Seism. Soc. Am.,* 90, 4,1041–1051

Margerin, L., Campillo, M., & van Tiggelen, B., 1998. Radiative transfer and diffusion of waves in a layered medium: new insight into coda Q, *Geophys. J. Int.,* **134**(2), 596–612.

Mayeda, K., Koyanagi, S., Hoshiba, M., Aki, A., & Zeng, Y., 1992. A Comparative-Study of Scattering, Intrinsic, and Coda Q^{-1} for Hawaii, Long Valley, and Central California Between 1.5-Hz and 15.0-Hz, *J. Geophys. Res.,* **97**, 6643–6659.

Meirova, T. & Pinsky, V., 2014. Seismic wave attenuation in Israel region estimated from the multiple lapse time window analysis and S-wave coda decay rate, *Geophys. J.Int.,* **197**, 581-590, doi: 10.1093/gji/ggu005.

Miller, S.A., Collettini, C., Chiaraluce, L., Cocco, M., Barchi. M, & Boris. J. P. K., 2004. Aftershocks driven by a high-pressure CO2 source at depth, *Nature,* **427**, 724 – 727.

Mongelli, F., Minelli, G., & Loddo, M., 2006. Geodynamics, thermal structure and depth of the brittle and semi-brittle layers in the Northern Apennine (Italy), *Boll. Geofis. Teor. Appl.,* **47**(3A), 375–399.

Mukhopadhyay, S., Kumar, A., Garg, A., Del Pezzo, E., & Kayal, J.R., 2014. The attenuation mechanism of S-waves in the source zone of the 1999 Chamoli earthquake*, Journal of Asian Earth Sciences,* **79**, 446–454.

Mukhopadhyay, S., Sharma, J., Del Pezzo, E., & Kumar, N., 2010. Study of Attenuation Mechanism for Garwhal–Kumaun Himalayas from Analysis of Coda of Local Earthquakes, *Phys. Earth Planet. Int.,* **180**, 7–15.

Paasschens, J., 1997. Solution of the time-dependent Boltzmann equation, *Phys. Rev. E.,* **56**, 1135–1141.

Padhy, S., & Subhadra, N., 2013. Separation of intrinsic and scattering seismic wave attenuation in Northeast India, *Geophys. J.Int.,* **195**(3):1892-1903.doi:10.1093/gji/ggt350.

Pauselli, C., Barchi, M., Federico, C., Magnani, M., & Minelli, G., 2006. The crustal structure of the Northern Apennines (Central Italy): an insight by the Crop03 seismic line, *Am. J. Sci.,* **306**, 428–450.

Piana Agostinetti, N., Lucente, F.P., Selvaggi, G., & Di Bona, M., 2002. Crustal structure and Moho geometry beneath the Northern Apennines (Italy), *Geophys. Res. Lett.,* **29**(20), doi:10.1029/2002GL015109.

Rovelli, A., Bonamassa, O., Cocco, M., Di Bona, M., & Mazza, S., 1988. Scaling laws and spectral parameters of the ground motion in active extensional areas of Italy, *Bull. Seism Soc. Am.*, 78, 530-560.

Sahin, S., Erduran, M., Alptekin, O., & Cakir, O., 2007. Intrinsic and scattering seismic attenuation in southewestern Anatolia, *Pure Appl. Geophys.,* **164**, 2255–2270, DOI 10.1007/ s00024-007-0263-

y.

Sato, H., 1977. Energy propagation including scattering effects: Single isotropic scattering approximation, J. Phys. Earth, ***25***, 27–41

Sato, H., & Fehler, M.C., 1998. *Seismic wave propagation and scattering in the heterogeneous Earth Springer*, New York.

Sawazaki, K., & Enescu, B., 2014. Imaging the high-frequency energy radiation process of a main shock and its early aftershock sequence: The case of the 2008 Iwate-Miyagi Nairiku earthquake, Japan, *J. Geophys. Res. Solid Earth,* **119**, doi:10.1002/2013JB010539.

Tselentis, G.A., 1998. Intrinsic and scattering seismic attenuation in W. Greece, *Pure Appl. Geophys.,* **153**, 703–712.

Tuvè, T., Bianco, F., Ibanez, J.M., Patanè, D., Del Pezzo, E., & Bottari, A., 2006. Attenuation study in the Straits of Messina area (southern Italy), *Tectonophysics,* **421**(3-4), 173–185.

Ugalde, A., Carcolè, E., & Vargas, C.A., 2010. S-wave attenuation characteristics in the Galeras volcanic complex (south western Colombia), *Phys. Earth Plan. Int.*, **183**, 73-81, doi:10.1016/j.pepi.2010.04.009.

Ugalde, A., Pujades, L.G., Canas, J.A. & Villasenor, A., 1998. Estimation of the intrinsic absorption and scattering attenuation in northeastern Venezuela (southeastern Carribean) using coda, *Pure Appl. Geophys.,* **105**, 685–702.

Ugalde, A., Tripathi, J.N., Hoshiba, M., & Rastogi, B.K., 2007. Intrinsic and scattering attenuation in Western India from aftershocks of the 26 January, 2001 Kachchh earthquake, *Tectonophysics,* **429**(1–2), 111–123.

Vargas, C.A., Ugalde, A., Pujades, L.G., & Canas, J.A., 2004. Spatial variation of coda wave attenuation in northwestern Columbia, *Geophys. J. Int.,* **158**, *609-624.*

Wennerberg, L., 1993. Multiple-scattering interpretations of coda-Q measurements, *Bull. Seism. Soc. Am.*, **83**, 279-290.

Yoshimoto, K., 2000. Monte Carlo simulation of seismogram envelopes in scattering media, *J.*

Geophys. Res., **105**, 6153–6161.

Yoshimoto, K., & Okada, M., 2009. Frequency-dependent attenuation of S-waves in the Kanto region, Japan, *Earth Planets Space,* **61**, 1067-1075.

Figure 1

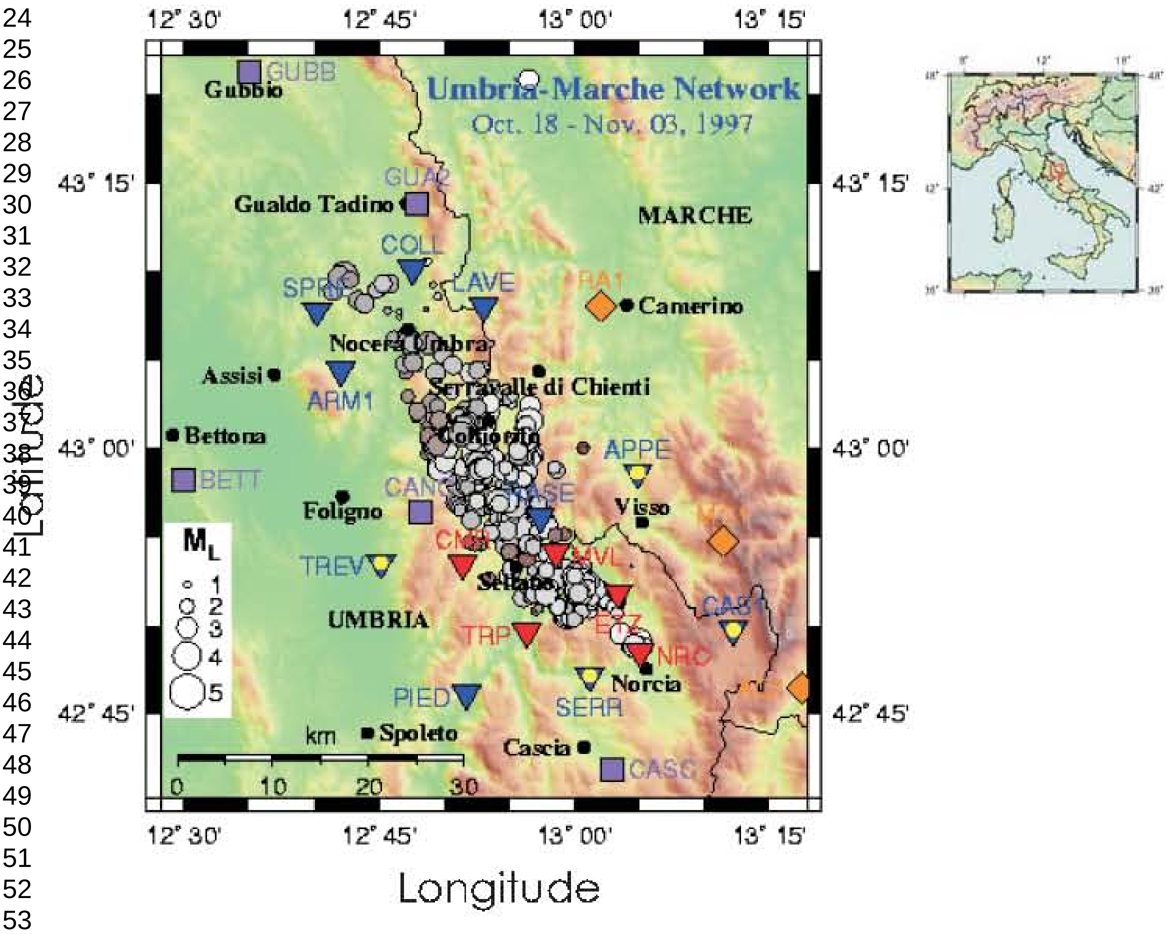
Umbria-Marche Network
Oct. 18 - Nov. 03, 1997
12° 30'
12° 45'
13° 00'
13° 15'
43° 15'
43° 00'
42° 45'
Longitude
Latitude
GUBB
Gubbio
GUA2
Gualdo Tadino
MARCHE
COLL
SPRI
LAVE
RA1
Camerino
Nocera Umbra
Assisi
ARM1
Serravalle di Chienti
Bettona
Colfiorito
APPE
BETT
CANC
CASE
Foligno
Visso
M_L
1
2
3
4
5
TREV
CMB
MVL
Sellano
UMBRIA
CAS1
TRP
NRC
Norcia
PIED
SERR
km
Spoleto
Cascia
CASC
0
10
20
30

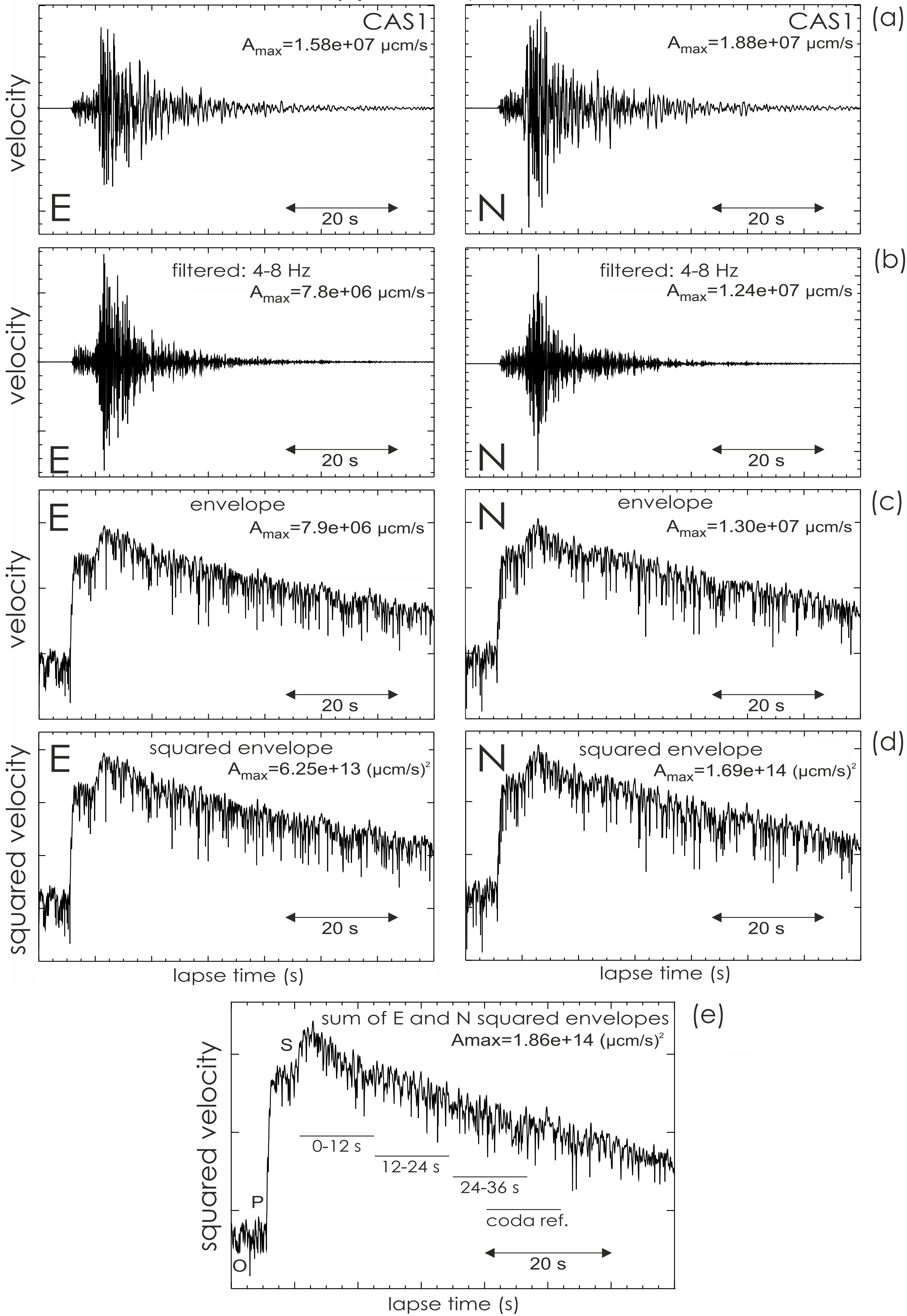
CAS1
A_{max}=1.58e+07 µcm/s
CAS1
A_{max}=1.88e+07 µcm/s
(a)
velocity
E
N
20 s
filtered: 4-8 Hz
A_{max}=7.8e+06 µcm/s
filtered: 4-8 Hz
A_{max}=1.24e+07 µcm/s
(b)
envelope
A_{max}=7.9e+06 µcm/s
envelope
A_{max}=1.30e+07 µcm/s
(c)
squared envelope
A_{max}=6.25e+13 (µcm/s)^2
squared envelope
A_{max}=1.69e+14 (µcm/s)^2
(d)
squared velocity
lapse time (s)
sum of E and N squared envelopes
Amax=1.86e+14 (µcm/s)^2
(e)
S
P
O
0-12 s
12-24 s
24-36 s
coda ref.
20 s
squared velocity
lapse time (s)

figure 3

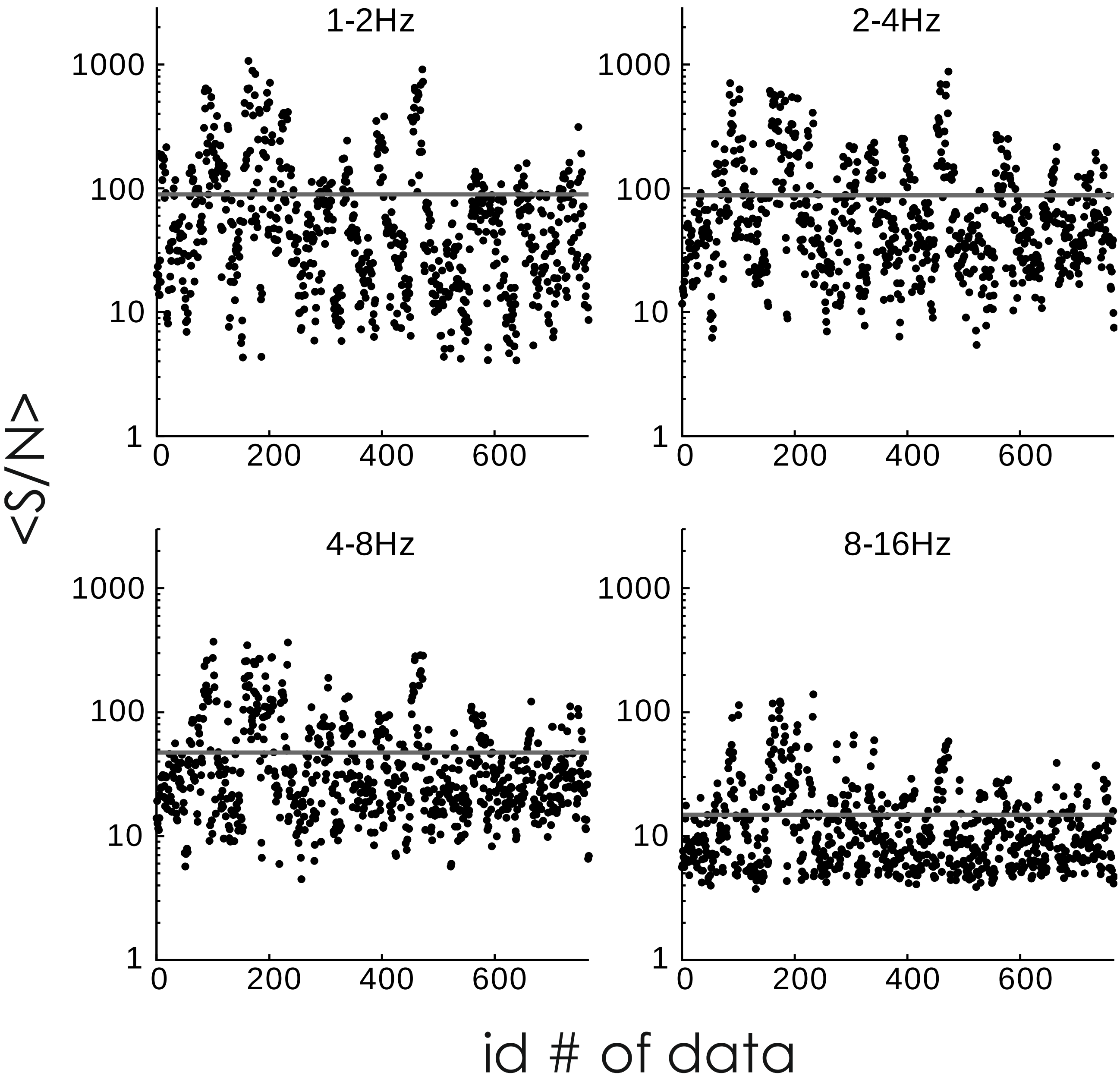

figure 4

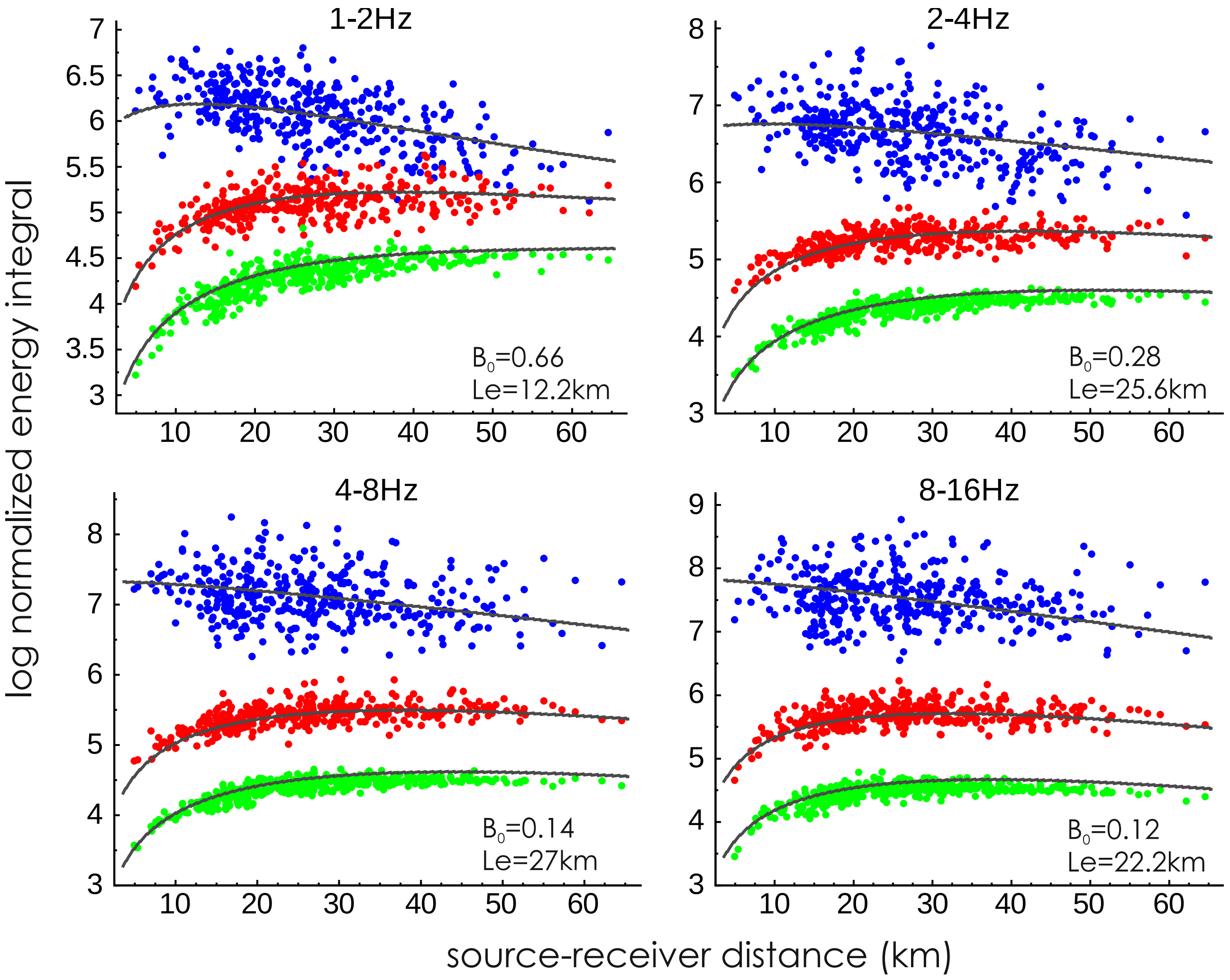

1-2Hz
2-4Hz
4-8Hz
8-16Hz
log normalized energy integral
source-receiver distance (km)
B0=0.66
Le=12.2km
B0=0.28
Le=25.6km
B0=0.14
Le=27km
B0=0.12
Le=22.2km

figure 5

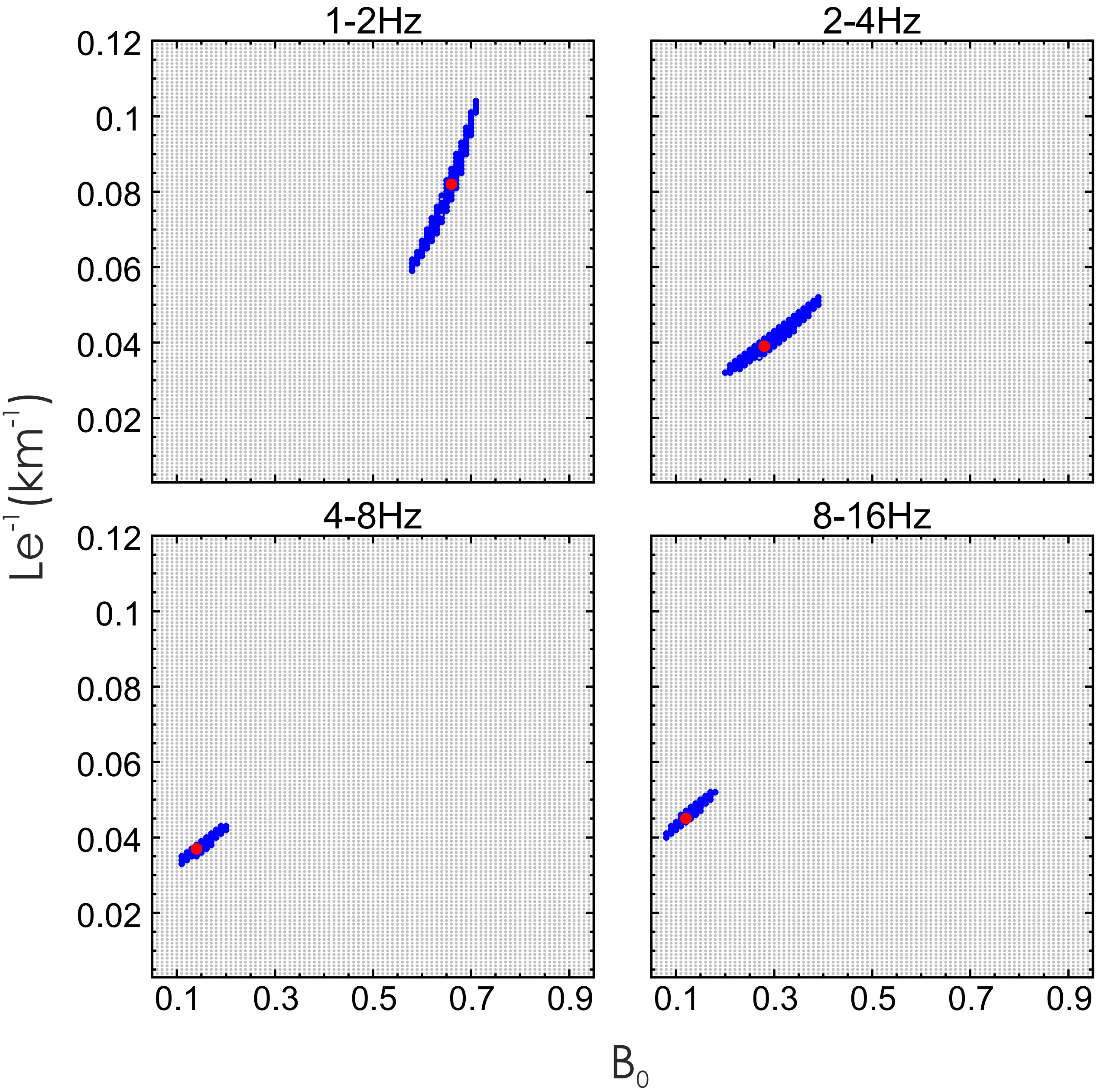
1-2Hz
2-4Hz
4-8Hz
8-16Hz
0.12
0.1
0.08
0.06
0.04
0.02
0.1 0.3 0.5 0.7 0.9
Le-1 (km-1)
B0

figure 6

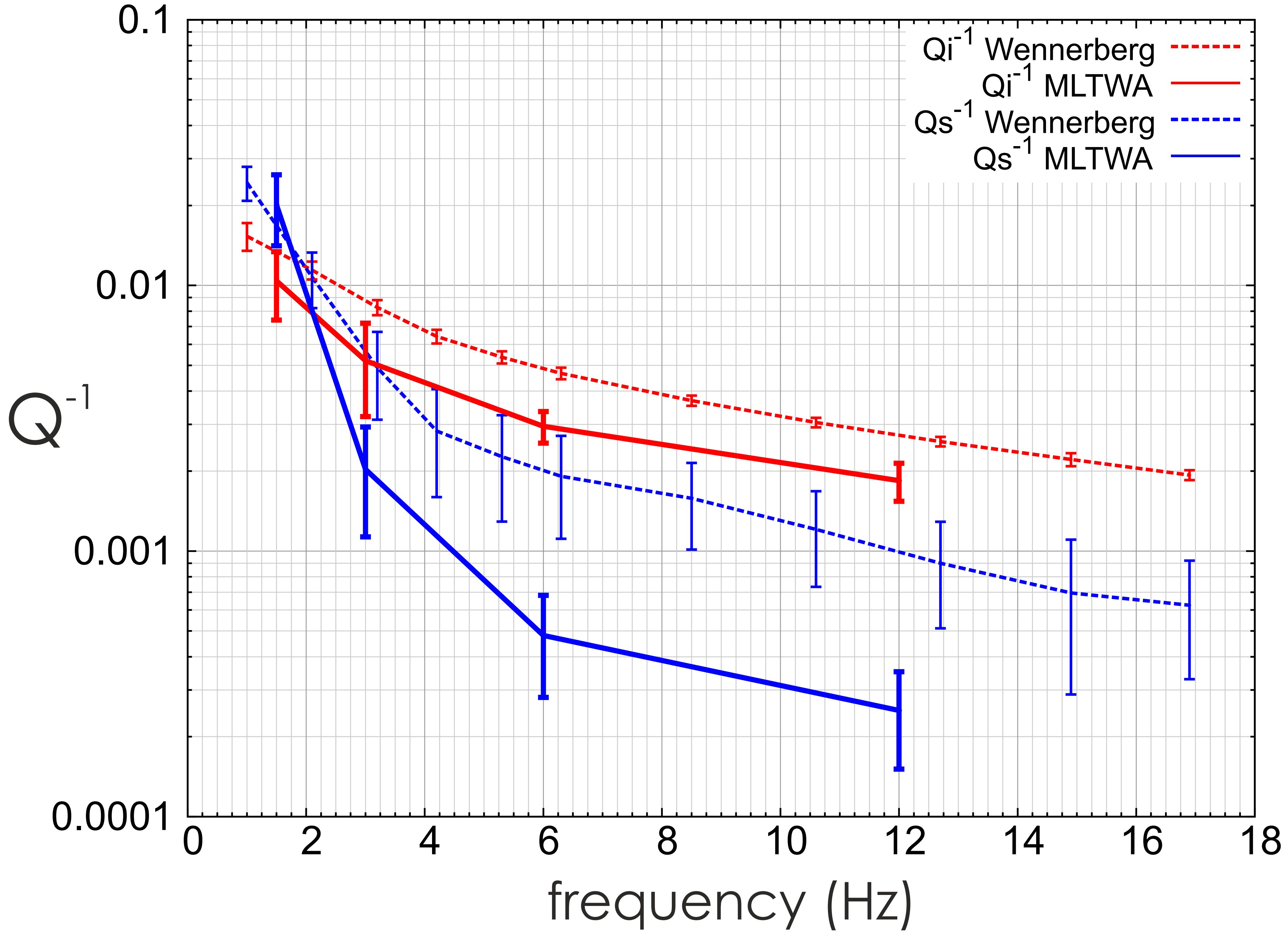
0.1
0.01
0.001
0.0001
0
2
4
6
8
10
12
14
16
18
frequency (Hz)
Q-1
Qi-1 Wennerberg
Qi-1 MLTWA
Qs-1 Wennerberg
Qs-1 MLTWA

figure 7

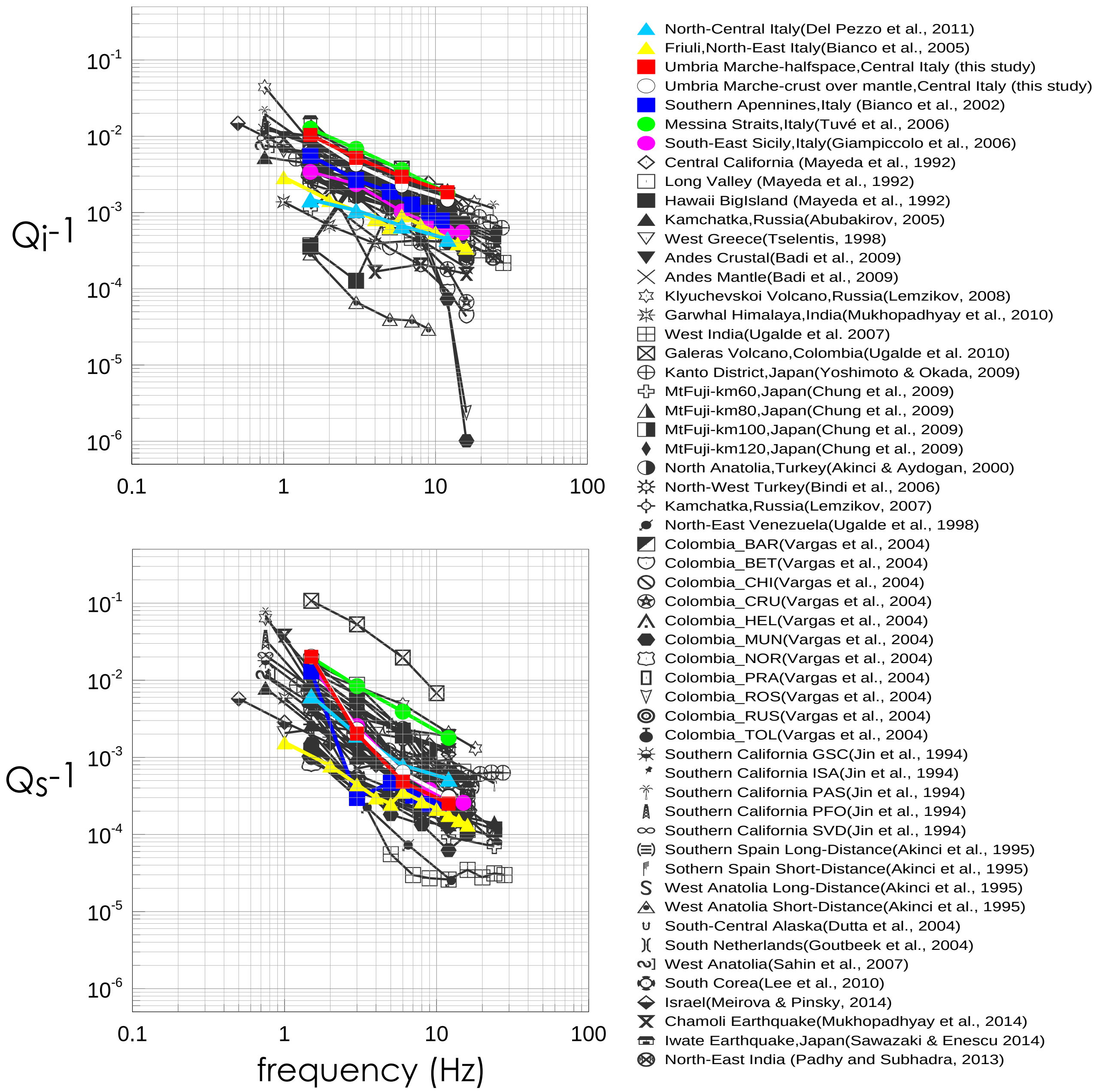
Qi-1
10-1
10-2
10-3
10-4
10-5
10-6
0.1
1
10
100
Qs-1
10-1
10-2
10-3
10-4
10-5
10-6
0.1
1
10
100
frequency (Hz)
North-Central Italy(Del Pezzo et al., 2011)
Friuli,North-East Italy(Bianco et al., 2005)
Umbria Marche-halfspace,Central Italy (this study)
Umbria Marche-crust over mantle,Central Italy (this study)
Southern Apennines,Italy (Bianco et al., 2002)
Messina Straits,Italy(Tuvé et al., 2006)
South-East Sicily,Italy(Giampiccolo et al., 2006)
Central California (Mayeda et al., 1992)
Long Valley (Mayeda et al., 1992)
Hawaii BigIsland (Mayeda et al., 1992)
Kamchatka,Russia(Abubakirov, 2005)
West Greece(Tselentis, 1998)
Andes Crustal(Badi et al., 2009)
Andes Mantle(Badi et al., 2009)
Klyuchevskoi Volcano,Russia(Lemzikov, 2008)
Garwhal Himalaya,India(Mukhopadhyay et al., 2010)
West India(Ugalde et al. 2007)
Galeras Volcano,Colombia(Ugalde et al. 2010)
Kanto District,Japan(Yoshimoto & Okada, 2009)
MtFuji-km60,Japan(Chung et al., 2009)
MtFuji-km80,Japan(Chung et al., 2009)
MtFuji-km100,Japan(Chung et al., 2009)
MtFuji-km120,Japan(Chung et al., 2009)
North Anatolia,Turkey(Akinci & Aydogan, 2000)
North-West Turkey(Bindi et al., 2006)
Kamchatka,Russia(Lemzikov, 2007)
North-East Venezuela(Ugalde et al., 1998)
Colombia_BAR(Vargas et al., 2004)
Colombia_BET(Vargas et al., 2004)
Colombia_CHI(Vargas et al., 2004)
Colombia_CRU(Vargas et al., 2004)
Colombia_HEL(Vargas et al., 2004)
Colombia_MUN(Vargas et al., 2004)
Colombia_NOR(Vargas et al., 2004)
Colombia_PRA(Vargas et al., 2004)
Colombia_ROS(Vargas et al., 2004)
Colombia_RUS(Vargas et al., 2004)
Colombia_TOL(Vargas et al., 2004)
Southern California GSC(Jin et al., 1994)
Southern California ISA(Jin et al., 1994)
Southern California PAS(Jin et al., 1994)
Southern California PFO(Jin et al., 1994)
Southern California SVD(Jin et al., 1994)
Southern Spain Long-Distance(Akinci et al., 1995)
Sothern Spain Short-Distance(Akinci et al., 1995)
West Anatolia Long-Distance(Akinci et al., 1995)
West Anatolia Short-Distance(Akinci et al., 1995)
South-Central Alaska(Dutta et al., 2004)
South Netherlands(Goutbeek et al., 2004)
West Anatolia(Sahin et al., 2007)
South Corea(Lee et al., 2010)
Israel(Meirova & Pinsky, 2014)
Chamoli Earthquake(Mukhopadhyay et al., 2014)
Iwate Earthquake,Japan(Sawazaki & Enescu 2014)
North-East India (Padhy and Subhadra, 2013)

figure 8

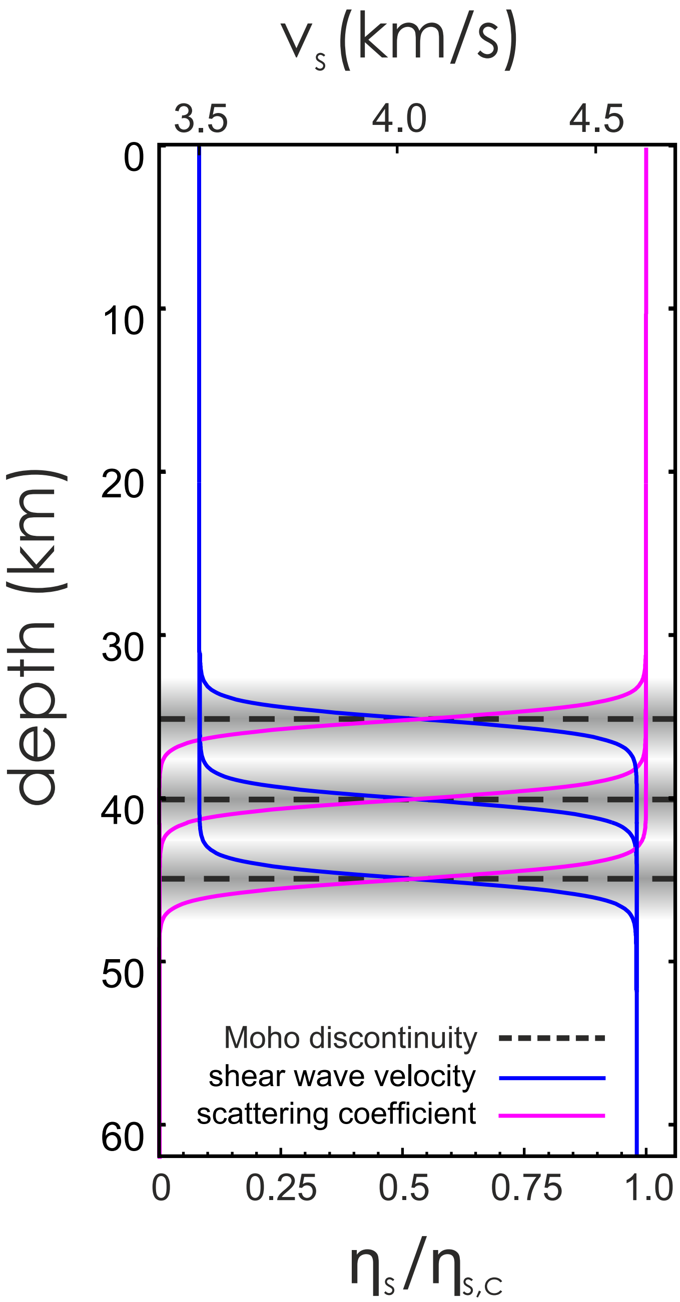

v_s (km/s)
3.5
4.0
4.5
depth (km)
0
10
20
30
40
50
60
Moho discontinuity
shear wave velocity
scattering coefficient
0
0.25
0.5
0.75
1.0
$\eta_s/\eta_{s,c}$

figure 9

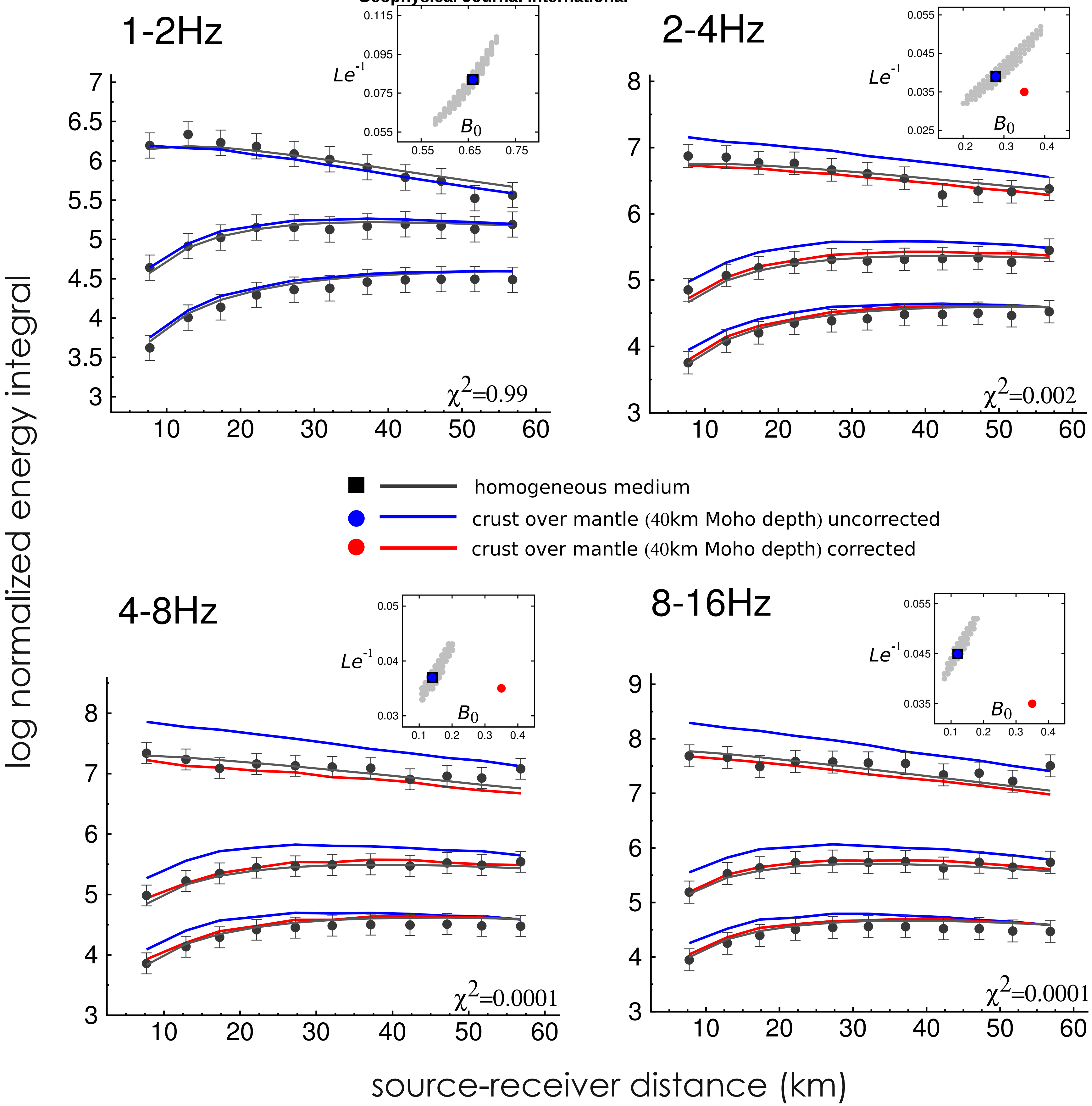
1-2Hz
2-4Hz
4-8Hz
8-16Hz
Le^{-1}
B_0
χ^2=0.99
χ^2=0.002
χ^2=0.0001
χ^2=0.0001
homogeneous medium
crust over mantle (40km Moho depth) uncorrected
crust over mantle (40km Moho depth) corrected
log normalized energy integral
source-receiver distance (km)

figure 10

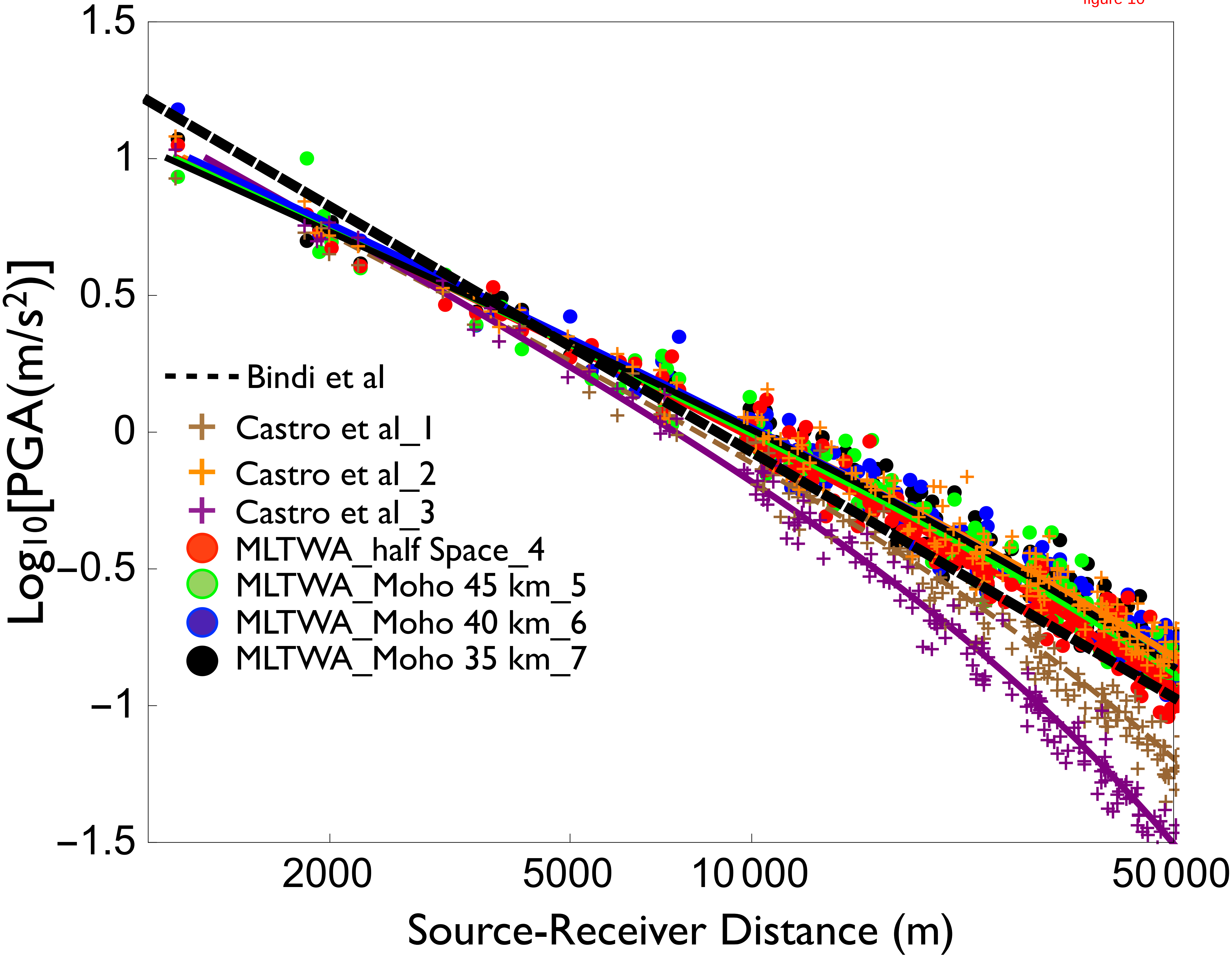
1.5
1
0.5
0
−0.5
−1
−1.5
Log10[PGA(m/s2)]
2000
5000
10 000
50 000
Source-Receiver Distance (m)
Bindi et al
Castro et al_1
Castro et al_2
Castro et al_3
MLTWA_half Space_4
MLTWA_Moho 45 km_5
MLTWA_Moho 40 km_6
MLTWA_Moho 35 km_7

Table I

Del Pezzo and Zollo (1984)

f(Hz)	Q_β
0.5	40
1	74
2	99
4	142
8	246
12	330
18	469
24	500
36	803

Rovelli et al., (1988)

$Q_\beta(f) = 100(f/f_0)^1$

Malagnini and Herrmann (2000)

$Q_\beta(f) = 130(f/f_0)^{0.1}$

Castro et al., (2002)

$Q_\beta(f) = 18(f/f_0)^2$ 1<f<10Hz

$Q_\beta(f)$ =900 f>10Hz

$Q_\beta(f) = 34(f/f_0)^{1.3}$

$Q_c(f) = 77(f/f_0)^{0.6}$

Bindi et al ., (2004)

$Q_\beta(f) = 49(f/f_0)^{0.9}$ $0.5 < f < 8Hz$

$Q_\beta(f) = 318$ $f > 8Hz$

Bindi et al., (2001)

$Q_0^{(**)}$	*n*	*station*
83	0.6	APPE
96	0.7	ARM1
87	0.7	CAS1
64	0.8	COLL
93	0.7	LAVE
68	0.7	RASE
81	0.7	SPRE
74	0.7	TREV

de Lorenzo et al., (2010)

$Q_0^{(*)}$	*n*	*station*
19	0.61	APPE
44	0.37	AQ1
20	0.65	ARM1
40	0.47	BETT
6	0.57	CANC
11	0.59	CAS1
41	0.34	CASC
8	0.66	CMR
13	0.67	COLL
24	0.35	ETZZ
59	0.29	GUA1
47	0.42	GUBB
51	0.44	LAVE
12	0.49	MC1
9	0.63	MVL
17	0.56	NRC
21	0.55	PIED
13	0.5	RA1
12	0.65	RASE
19	0.56	SERR
18	0.73	SPRE
15	0.53	TREV
15	0.52	TRP

de Lorenzo et al., (2013a)

f(Hz)	Q_c	Q_β	Q_s	Q_i
1	88	25	40	61
2.1	104	45	92	83
3.2	137	76	204	118
4.2	172	108	353	153
5.3	205	131	441	183
6.3	235	152	523	211
8.5	298	190	633	267
10.6	358	235	828	32
12.7	419	287	1111	382
14.9	487	344	1437	447
16.9	558	391	1600	511

de Lorenzo et al., (2013b)

f(Hz)	Q_α	Q_β
1.5	12	20
4	16	59
8	30	94
14	65	246
24	360	415

* $Q_\alpha(f) = Q_0(f/f_0)^n$

** $Q_\beta(f) = Q_0(f/f_0)^n$

$(f_0 = 1Hz)$

Table II

f(Hz)	*rms*	B_0	δB_0	Le^{-1} (km^{-1})	δLe^{-1} (km^{-1})	Q_i^{-1}	δQ_i^{-1}	Q_s^{-1}	δQ_s^{-1}	Q_t	δQ_t
1.5	42.5	0.66	0.07	0.082	0.023	1.04E-02	3.00E-03	2.01E-02	6.00E-03	33	8
3	59.2	0.28	0.1	0.039	0.01	5.21E-03	2.00E-03	2.03E-03	9.00E-04	138	38
6	59.8	0.14	0.05	0.037	0.005	2.95E-03	4.00E-04	4.81E-04	2.00E-04	291	42
12	78.2	0.12	0.05	0.045	0.006	1.84E-03	3.00E-04	2.51E-04	1.00E-04	478	69

Table III

	band pass 1-2Hz				*band pass 2-4Hz*			
model	Q_i	Q_s	B_0	Le^{-1} (km^{-1})	Q_i	Q_s	B_0	Le^{-1} (km^{-1})
halfspace	97	50	0.66	8.20E-02	192	493	0.28	3.90E-02
45km Moho depth	97	50	0.66	8.20E-02	220	467	0.32	3.60E-02
40km Moho depth	97	50	0.66	8.20E-02	237	440	0.35	3.50E-02
35km Moho depth	97	50	0.66	8.20E-02	247	440	0.36	3.40E-02
	band pass 4-8Hz				***band pass 8-16Hz***			
halfspace	339	2079	0.14	3.70E-02	544	3989	0.12	4.50E-02
45km Moho depth	421	1683	0.2	3.20E-02	658	3452	0.16	3.90E-02
40km Moho depth	445	1579	0.22	3.10E-02	683	3335	0.17	3.80E-02
35km Moho depth	466	1561	0.23	3.00E-02	710	3235	0.18	3.70E-02

Table IV

Seismic Moment M_0 (N·m)	*Magnitude M_L*	*Stress-Drop $\Delta\sigma$ (Pa)*	*Spectral decay parameter k (s)*	*Corner frequency fc (Hz)*
$3.5 \cdot 10^{16}$	5.0	$7 \cdot 10^{6}$	0.05	0.8